Nonlinear Dyn (2022) 110:3015–3030
https://doi.org/10.1007/s11071-022-07793-w

ORIGINAL PAPER

Nonlinear dynamics of a bistable system impacting a sinusoidally vibrating shaker

Michael Rouleau · Steven Craig · Yiwei Xia · Roy Shieh · Major L. Robinson · Chengzhi Shi · Julien Meaud

Received: 5 February 2022 / Accepted: 8 August 2022 / Published online: 2 September 2022

Abstract Bistable systems have seen significant interest in recent years, in applications ranging from energy harvesting, impact mitigation, and aerospace, to precision sensing and metamaterials. However, most investigations of bistable systems consider only continuous external forcing. The literature on the topic of vibroimpact dynamics is vast, but is mostly limited to monostable systems. In this work, we advance the state of knowledge by considering the fundamental problem of a one degree-of-freedom bistable system subjected to vibroimpact forcing by a sinusoidally vibrating shaker. Using computational models, we find that by varying excitation amplitude and frequency, a rich nonlinear dynamic behavior can be observed. Some responses exhibit only intrawell dynamics, while others display interwell motion that may converge to a second equilibrium. Analytical equations are derived to estimate the amplitude threshold that corresponds to the excitation amplitude required to observe interwell motion. The influence of the excitation frequency on the nonlinear dynamics of the system includes the presence of a local minimum in the threshold which is linked to a nonlinear resonance of the system. Further, response types can be differentiated by aperiodic (including chaotic) and periodic responses that include responses of periods one through six. In addition to computational simulations, the existence and stability of periodic orbits are determined using a shooting method based on the response over a single cycle. Experimental work using a magnetic bistable pendulum qualitatively validates the theoretical findings.

Keywords Vibrodynamics · Bistability · Nonlinear dynamics · Impact forcing

Supplementary Information The online version contains supplementary material available at https://doi.org/10.1007/s11071-022-07793-w.

M. Rouleau · S. Craig · Y. Xia · R. Shieh · M. L. Robinson · C. Shi · J. Meaud (✉)
G.W.W. School of Mechanical Engineering, Georgia Institute of Technology, 771 Ferst Drive, Atlanta, GA 30332, USA
e-mail: julien.meaud@me.gatech.edu

1 Introduction

Systems including one or more bistable mechanical systems, which exhibit two stable equilibria, have been under extensive research in recent years, particularly in the areas of metamaterials [1–3] and energy harvesting [4–6], or even mechanical computing [7]. Bilal et al. [8] investigated bistable elements as a means for switching between two states, while Xia et al. [9] explored the influence of system parameters on escape from energy wells using base excitation. The propagation of transition waves in 1D chains of bistable elements has been studied by Raney et al. [10]. Harmonic displacement constraints have also been considered by the likes of Arrieta et al. [11], who use a shaker to prescribe the displacement of a portion of the structure. Textbooks such as those by Virgin, Wang et al., and

Datseris et al. explore fundamental bistable systems with numerous applications but neglect the case of impact forcing [12–14]. These studies allow for precise tuning of energy harvesters and metastructures subject to base excitation, harmonic displacement, or quasi-static actuation. However, the literature regarding vibroimpact forcing on bistable systems, where excitation is provided by collisions with a harmonically displaced barrier, is more limited. Considering this type of excitation is essential for incorporating bistable structures into mechanisms and assemblies, with applications spanning switching, sensing, and energy harvesting.

Impact-forced systems exhibit highly nonlinear and nonsmooth dynamics and are frequently found in machines and mechanisms. Previous studies have extensively explored classical systems such as balls bouncing on vibrating surfaces [15] or flexible beams [16] and nonlinear systems under continuous external forcing [17–19]. Additionally, displacement constraints have been studied in conjunction with base excitation or continuous external forcing [20–22]. In particular, Gu and Livermore showed a linear system subjected to impact displays rich dynamics [22]. While many of these studies highlight nonlinearities present from impacts or the underlying system, few consider the fundamental issue of a bistable system driven solely by collisions. A notable exception is the work of Xie et al., who studied a piezoelectric bistable system with a unilateral displacement constraint [23]. Xie et al., however, focused on the analysis of their system for its application as an energy harvester rather than a study of the fundamental nonlinear dynamics of the system.

While prior investigations consider impact excitation and bistable systems independently, few studies have focused on the combined nonlinear dynamics. The current work investigates a fundamental class of systems represented by an inherently bistable single degree of freedom (SDOF) system driven by collisions with a sinusoidally vibrating shaker. Theoretical and experimental results are presented to analyze the fundamental nonlinear dynamics of the system. Such a system displays complex frequency and amplitude-dependent dynamics with intrawell and either transient or continuous interwell oscillations. The present work explores these complex dynamics with the goal of classifying the possible dynamic responses and identifying which conditions are required to achieve them. After deriving a numerical model, we focus on varying excitation frequency and amplitude to explore the response types and some associated bifurcations. Finally, we show experimental results which indicate our model is capable of predicting these physical phenomena.

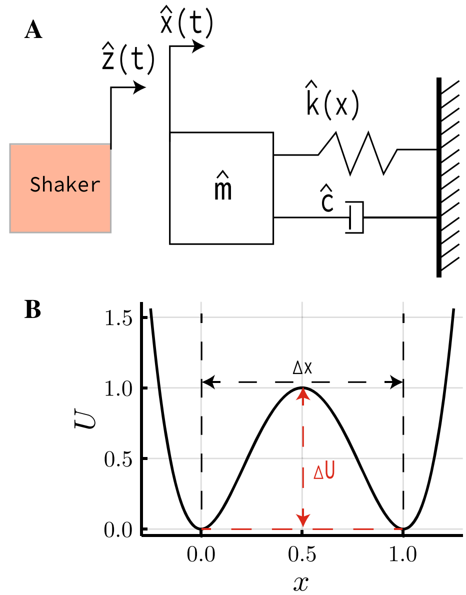

Fig. 1 **a** Lumped system with dimensional parameters. **b** Bistable potential energy profile. Δx is the distance between energy minima, and ΔU is the energy barrier

2 Model for the impact-forced dynamics of a bistable system

The single degree of freedom is represented as the lumped parameter system as shown in Fig. 1. A mass $\hat{m}$ of displacement $\hat{x}$ attached to a bistable spring of nonlinear stiffness $\hat{k}(\hat{x})$ and viscous damping coefficient $\hat{c}$, where $\hat{}$ denotes dimensional quantities. The system is initially at rest ($\hat{x}(0) = 0$, $\frac{\partial \hat{x}}{\partial \hat{t}}(0) = 0$). When this system is subjected to a time-dependent displacement constraint $\hat{z}(\hat{t})$ with initial contact, $\hat{x}(\hat{t}) \geq \hat{z}(\hat{t})$, the system undergoes one or more collisions with the shaker, which is prescribed velocity of the form $\hat{v}(\hat{t}) = \hat{V}\cos(\hat{\Omega}\hat{t})$ for $\hat{t} > 0$, where $\hat{V}$ is the shaker velocity amplitude and $\hat{\Omega}$ is the frequency of oscillation.

2.1 Governing equations

The bistable spring is assumed to have equal energy minima (Fig. 1b), such that the potential energy can be expressed as:

$$\hat{U}(\hat{x}) = \frac{1}{2}\hat{k}_0\hat{x}^2\left(1 + \frac{\hat{x}^2}{\Delta\hat{x}^2} - 2\frac{\hat{x}}{\Delta\hat{x}}\right) \quad (1)$$

Here, $\hat{k}_0$ refers to the spring's linear stiffness and $\Delta\hat{x}$ is the distance between the two equilibrium positions. Between collisions, the equation of motion of the system is:

$$\hat{m}\frac{\partial^2\hat{x}}{\partial\hat{t}^2} + \hat{c}\frac{\partial\hat{x}}{\partial\hat{t}} + \frac{\partial\hat{U}}{\partial\hat{x}} = 0 \quad (2)$$

Collisions are handled instantaneously via the coefficient of restitution, e, which relates the mass's velocity immediately before and after a collision according to the equation:

$$\left.\frac{\partial\hat{x}}{\partial\hat{t}}\right|_{\hat{t}_n^+} = -e\left.\frac{\partial\hat{x}}{\partial\hat{t}}\right|_{\hat{t}_n^-} + (1+e)\left.\frac{\partial\hat{z}}{\partial\hat{t}}\right|_{\hat{t}_n}, \quad (3)$$

where $\hat{z}$ is the shaker displacement and $\hat{t}_n$ is the time at the nth impact. The governing equations can be written in the following non-dimensional form:

$$\frac{\partial^2 x}{\partial t} + 2\zeta\frac{\partial x}{\partial t} + x - 3x^2 + 2x^3 = 0 \text{ if } x(t) > z(t) \quad (4)$$

$$\left.\frac{\partial x}{\partial t}\right|_{t_n^+} = -e\left.\frac{\partial x^-}{\partial t}\right|_{t_n^-} + (1+e)\left.\frac{\partial z}{\partial t}\right|_{t_n} \text{ if } x(t_n) = z(t_n), \quad (5)$$

where the following non-dimensional quantities have been introduced:

$$t = \frac{\hat{\omega}_0}{2\pi}\hat{t} \quad x(t) = \frac{\hat{x}(\hat{t})}{\Delta\hat{x}} \quad z(t) = \frac{\hat{z}(\hat{t})}{\Delta\hat{x}}, \quad (6)$$

where $\hat{\omega}_0$ and ζ are the linear natural frequency and damping ratio of the system, respectively:

$$\hat{\omega}_0 = \sqrt{\frac{\hat{k}_0}{\hat{m}}} \quad \zeta = \frac{\hat{c}}{2\sqrt{\hat{m}\hat{k}_0}}. \quad (7)$$

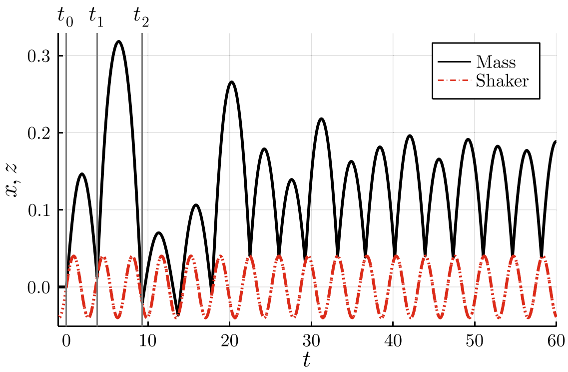

Fig. 2 An example waveform, with impacts occurring at $t_0, t_1, t_2, \ldots$. The transient response overshoots the steady-state amplitude before converging to a periodic solution

The following non-dimensional variables are used to define the frequency and velocity amplitude of the shaker:

$$\Omega = \frac{\hat{\Omega}}{\hat{\omega}_0} \quad V = \frac{\hat{V}}{\hat{\omega}_0 \times \Delta\hat{x}}. \quad (8)$$

Numerical simulations are conducted using the Julia programming language [24] and the *Vern9* 8th-/9th-order Runge–Kutta algorithm from the DifferentialEquations.jl package [25]. Each impact is handled via DifferentialEquations.jl's *ContinuousCallback* functionality. Each tolerance was decreased until the qualitative results described here were converged. All results except for Figs. 13 and 14 were obtained using $\zeta = 0.02$ and $e = 0.85$. An example of simulated waveform is shown in Fig. 2.

2.2 Handling of sticking phenomenon

As $\Omega \to 0$ for $e < 1$, it is possible for the mass and shaker to enter a series of close collisions termed "chatter" [26]. In the limiting case $\Omega = 0$, this becomes an infinite series of of collisions as the mass and shaker slowly converge to the same position. For simulation, such chatter is truncated when two collisions occur within $t < 10^{-9}$, after which the mass and shaker are assumed to remain in contact until the contact force becomes negative. This contact force corresponds to the value of the left hand side of Eq. (4) when $x(t) = z(t)$, which results in the condition to maintain sticking,

$$\frac{\partial^2 z}{\partial t} + 2\zeta\frac{\partial z}{\partial t} + z - 3z^2 + 2z^3 \geq 0. \quad (9)$$

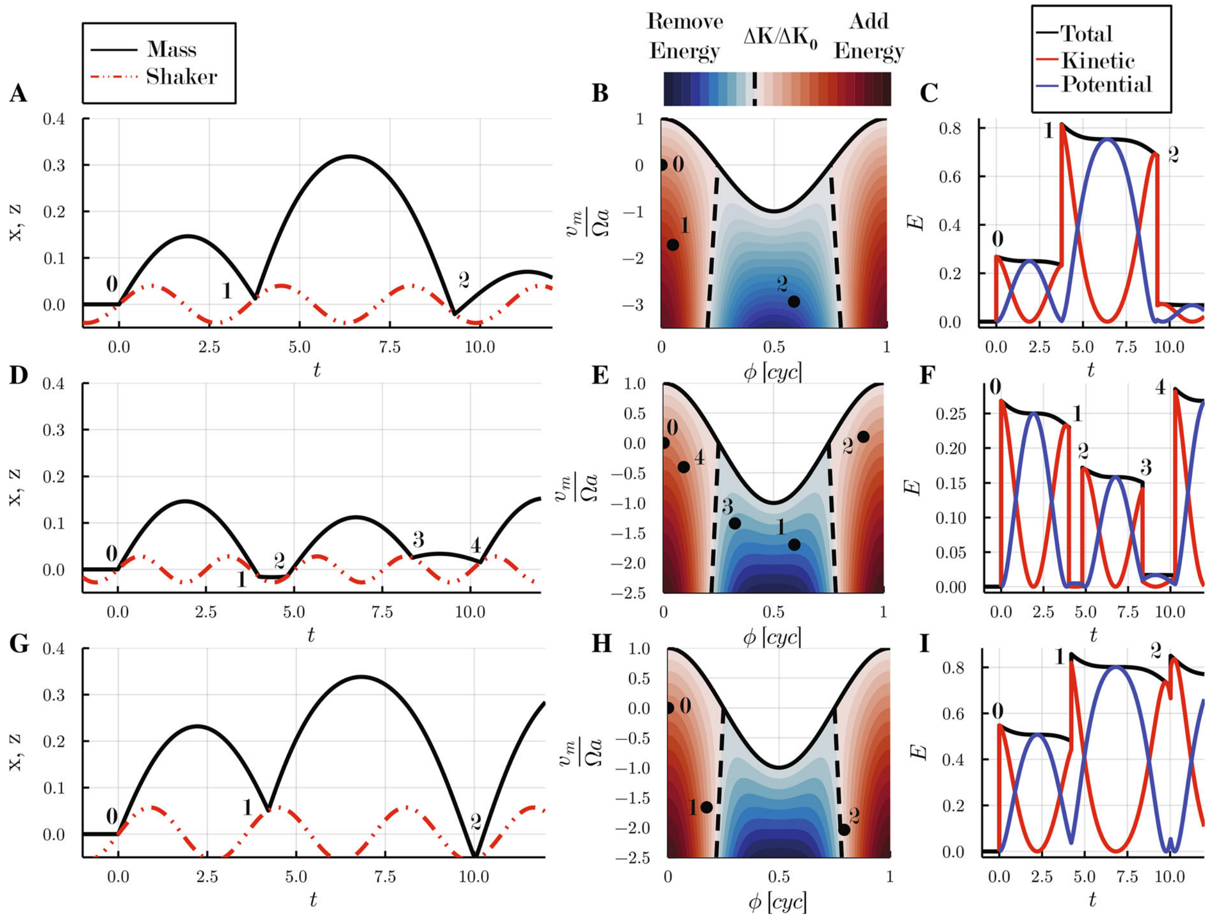

Fig. 3 Illustration of the effect of frequency on the first few response cycles. **a, d, g** Waveform immediately after $t = 0$. **b, e, h** Change in energy for each impact given by Eq. (13). The dashed line is the neutral line, which corresponds to no net energy change after impact. **c, f, i** Mass kinetic, potential, and total energy. Numbered square symbols indicate the first few impacts. Parameters: **a–c** $\Omega = 1.75,\ V = 0.07$, **d–f** $\Omega = 2.5,\ V = 0.07$. **g–i** $\Omega = 1.75,\ V = 0.10$. By maintaining maximum shaker velocity and varying frequency, the phase of impacts is varied. For the same velocity ($V = 0.07$) in **a–c** and **d–f**, solutions will be identical until the second impact, even though the frequencies differ

3 Analysis of the nonlinear dynamics of the system

3.1 Effect of frequency and velocity of the shaker on the initial response of the mass

Varying the non-dimensional frequency, Ω, or velocity amplitude, V, of the shaker excitation has very distinct effects on the response of the bistable system. Figure 3 illustrates the first few cycles of the response predicted by our model in a baseline case ($\Omega = 1.75$, $V = 0.07$) and cases with either increased frequency ($\Omega = 2.5$, $V = 0.07$), or increased amplitude ($\Omega = 1.75$, $V = 0.14$). The effect of these stimulus parameters on the response of the mass can be understood by examining the effect of each impact on the mass. A collision at time t_n causes a discontinuity in the kinetic energy according to:

$$\Delta K(t_n) = \frac{1}{2} m v(t_n^+)^2 - \frac{1}{2} m v(t_n^-)^2 \tag{10}$$

where v denotes the non-dimensional velocity ($v = \frac{\partial x}{\partial t}$). $v(t_n^+)$ is related to $v(t_n^-)$ by Eq. (5). The mass is at rest prior to the first collision at $t = 0$ such that:

$$\Delta K_0 = \frac{m\left[V(1+e)\right]^2}{2} \tag{11}$$

Because Eq. (11) does not depend on Ω, the responses for $t \leq t_1$ are identical when Ω is increased while V is kept constant (compare panel A to panel B of Fig. 3). However, because the shaker has a higher frequency, the second impact occurs at a different time. The timing of a collision, $\hat{t}_n$, can be used to define the phase of the impact according to:

$$\phi_n = \Omega \hat{t}_n \mod 2\pi \tag{12}$$

By this definition, the phase of the first impact is always set to be 0. The phase of the 2nd impact is $\phi_1 \approx 0.05$ cycles for $\Omega = 1.75$ and $\phi_1 \approx 0.59$ cycles for $\Omega = 2.5$. This change in the impact phase has important consequences on the effect of collisions on the energy of the system. The change of the energy for the nth collision can be expressed as a function of ϕ_n and of the velocity prior to the impact, $v(t_n^-)$:

$$\Delta K(t_n) = \Delta K_0 \left[\left(\cos \phi_n - \frac{e}{1+e} \frac{v(t_n^-)}{V} \right)^2 - \left(\frac{1}{1+e} \frac{v(t_n^-)}{V} \right)^2 \right] \tag{13}$$

A surface plot of the energy is plotted as function of ϕ_n and $v(t_n^-)$ in the center column of Fig. 3, which allows us to visualize the effect of these parameters on the energy change due to each collision. $\Delta K(t_n)$ can be positive (implying that the collision adds energy) or negative (implying that the collision removes energy) according to Eq. (13). The condition for a collision to add energy is

$$-\frac{1+e}{1-e} \cos \phi_n \leq \frac{v(t_n^-)}{V} \leq \cos \phi_n. \tag{14}$$

The first inequality yields the boundary shown in the dashed line in Fig. 3. We also note collision is only possible if $v(t_n^-) \leq \dot{z}(t_n)$, which yields the following inequality:

$$\frac{v(t_n^-)}{V} \leq \cos \phi_n \tag{15}$$

such that the energy is only plotted below the thick solid line in the figure. Impacts that occur on this line are termed grazing impacts. The points corresponding to the first few impacts are shown in the center column of Fig. 3. In agreement with these panels, we observe in the graph of the energy vs time that the 2nd collision removes energy in Panel D, while it adds energy in Panel A. Between each collision, potential and kinetic energy is exchanged, and the total energy decays due to viscous damping.

Increasing the velocity amplitude (3rd row of Fig. 3) increases ΔK_0 according to Eq. (11), such that the response between 1st and 2nd impact reaches a higher amplitude. This increase in the amplitude of the response results in a softening effect due to the nonlinearity of the spring, affecting both the phase of the 2nd collision, and the velocity at the time of the 2nd collision.

Changing the phase of the second collision and the energy added by the first collision by varying stimulus frequency or amplitude allows us to observe a very rich nonlinear dynamical behavior, which is explored in the next sections.

3.2 Transition to and out of chaos when Ω is varied

The steady-state response is investigated by simulating 20,000 linear natural periods of the system and categorizing responses based on periodicity and which energy well(s) the mass orbits near or converges to at the end of the simulations. We first study the influence of excitation frequency on the response for low amplitude shaker velocity.

3.2.1 Transition to chaos

For shaker excitations of low amplitude and frequency, the response remains around the first equilibrium. This intrawell response can be periodic with a period of $1, 2, \ldots, 6+$, or chaotic, as it passes through a series of bifurcation points as frequency changes. For example, Fig. 4 shows several stages in this transition: from period-one response to period-two to period-four to chaos as frequency increases.

In Fig. 4a–c, a period-one response is displayed, where the mass waveform repeats for each period of excitation. Figure 4a shows the steady-state waveform with a period which matches the excitation period and includes one impact per cycle. Figure 4b shows the state space portrait for many cycles of this response with the Poincaré section overlaid. The single path and point on the Poincaré section indicate a period of one while

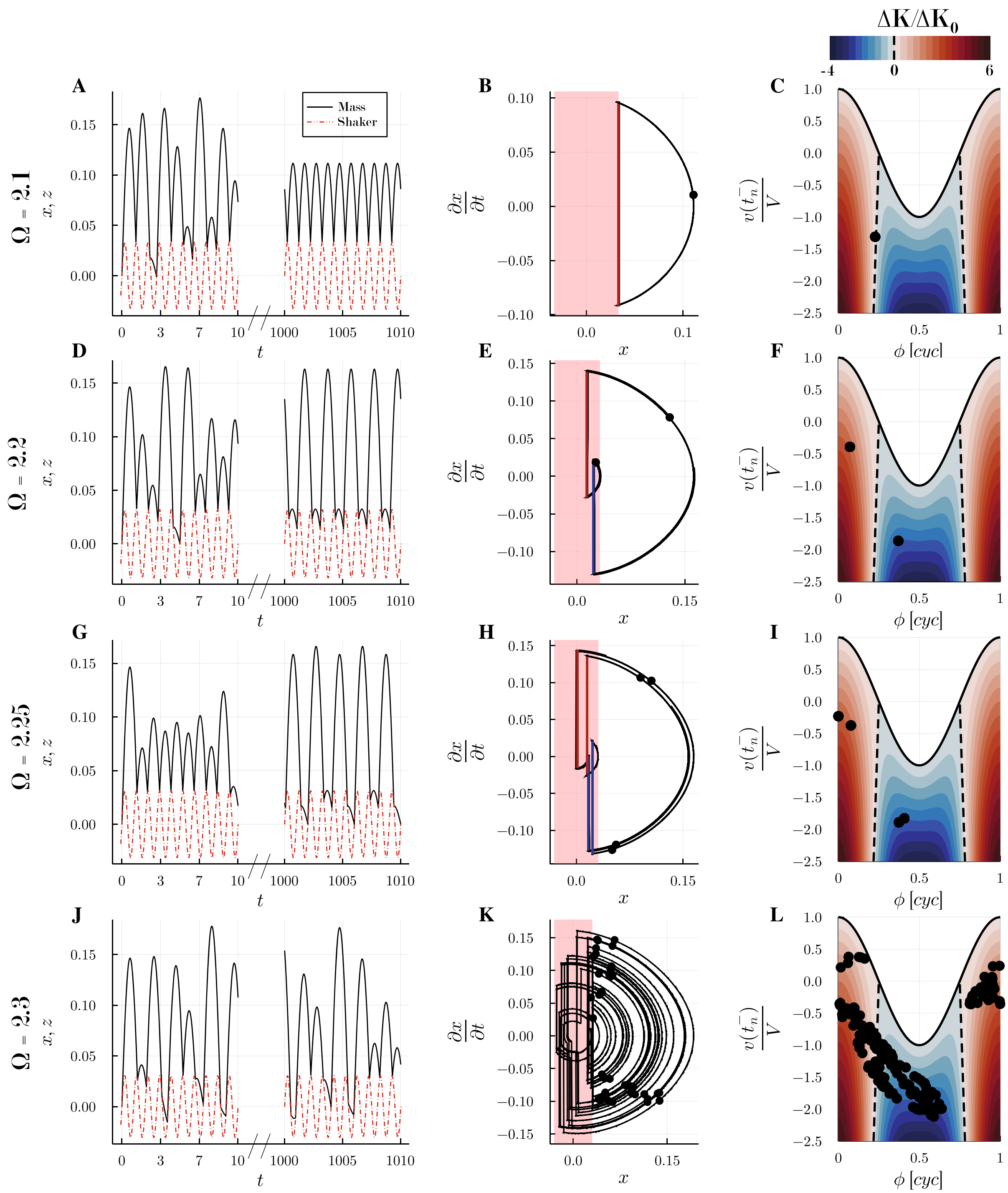

Fig. 4 Transition to chaos as frequency increases for $V = 0.07$. **a, d, g, j** Waveforms showing both transient and steady-state responses. **b, e, h, k** Phase plane with overlaid Poincaré section for steady-state response. The shaded region indicates the range of shaker displacement. The discontinuities highlighted in red in Panel **e, h** add energy while the blue discontinuities removes energy. **c, f, i, l** Change in energy for each steady-state impact given by Eq. (13). (Color figure online)

the single velocity discontinuity is the single impact per cycle. Figure 4c quantifies the energy added or lost for each impact at steady state. The impact occurs near the dotted line, which indicates it is adding very little energy per impact to compensate for viscous damping. For high values of e, this also corresponds to an impact occurring near the maximum or minimum shaker displacement. For a periodic solution to exist, the sum of the impacts must compensate for any energy lost.

Figure 4d–f shows a response which occurs at a slightly higher frequency. The waveform in Fig. 4d and the two points on the Poincaré section in Fig. 4e are consistent with a period-two periodic response. One impact per period of excitation, or equivalently, two impacts per cycle of the mass, corresponding to the discontinuities in the waveform and phase portrait, are observed. The impacts in Fig. 4f show that energy is added with an impact just before peak shaker displacement and is removed with an impact just after the peak. The sum of these energy transfers still adds energy to the mass. The phase of each impact has moved further from the neutral line.

Figure 4g–i shows a period-four response, with four impacts per cycle. Energy is alternately added and removed from the mass with each impact, with two impacts on each side of the neutral line.

The remaining panels in Fig. 4 show a chaotic response. The waveform in Fig. 4j has no repetition, and Fig. 4k shows approximately 100 cycles, each with its own path on the state space map and point in the Poincaré section. This chaos extends to the impact map in Fig. 4l, which shows impacts adding and removing energy, with impacts occurring over large regions of the map. The chaotic behavior of the response was confirmed by examining the spectrum of the response, which is broadband as seen in Fig. S2 in Supplemental Information. The shifting impact conditions described in Fig. 3 is one of the reasons for the transition to chaos. In particular, grazing impacts are a source of chaos in the system. Minor variations dictate whether the impact occurs or not, leading to large changes in the response.

3.2.2 Transition out of chaos

In another type of bifurcation, the system response can change dramatically as it moves into the second equilibrium. For example, Fig. 5 shows the effect of an even higher frequency of excitation with the same shaker velocity of $V = 0.07$. For this example, the system moves from a period-six response to period-three before reaching sufficient energy to move to the second equilibrium. After a region of chaos spanning $\Omega \approx 2.3 - 2.5$ described near the end of the preceding section, the system returns to a periodic response. In Fig. 5a, the system exhibits a period-six response, which agrees with the Poincaré section in Fig. 5b. Figure 5c highlights that the mass's impacts occur just before the shaker displacement extrema, adding energy near the maxima and removing energy near the minima. As frequency is increased slightly, the system converges to the period-three response in Fig. 5d. Although the period is three, only two impacts occur per cycle, as evidenced by the pair of discontinuities in Fig. 5e and the points in Fig. 5f. Once the mass has sufficient energy, the threshold is exceeded and the system shifts into the second equilibrium. The last few cycles before snapthrough are shown in Fig. 5g, while Fig. 5h, i describes the chaotic response that is observed before snapthrough.

3.2.3 Bifurcation diagrams

These bifurcations can be seen in greater detail in Fig. 6. In Fig. 6a, the maximum displacement per cycle of excitation is plotted against excitation frequency. Between $\Omega = 2$ and $\Omega \approx 2.15$, the maximum amplitude decreases monotonically as the system limits the softening effect of the bistable spring in order to maintain stability at higher frequencies. In the same region, Fig. 6b shows a slowly increasing phase toward $\phi = 0.25$ cycles which corresponds to lower energy added for each impact. After the first bifurcation shown, two branches of both maximum displacement and phase become visible, indicating a period-doubling effect and one impact per period of excitation. Near $\Omega = 2.25$, a second bifurcation occurs, doubling the period again, into a period-four response. As frequency increases past $\Omega \approx 2.3$, chaos emerges in the system. This period-doubling bifurcation into chaos is also observed in quasi-linear impact systems and is typical of strange attractors [27].

A shooting method based on the computation of a single cycle of the response was used as alternative method to determine periodic solutions. This shooting method, which was adapted from [28,29] and is described in Supplemental Information, can also be used to establish the stability of periodic solutions by examining the Floquet multipliers, i.e., the eigenvalues

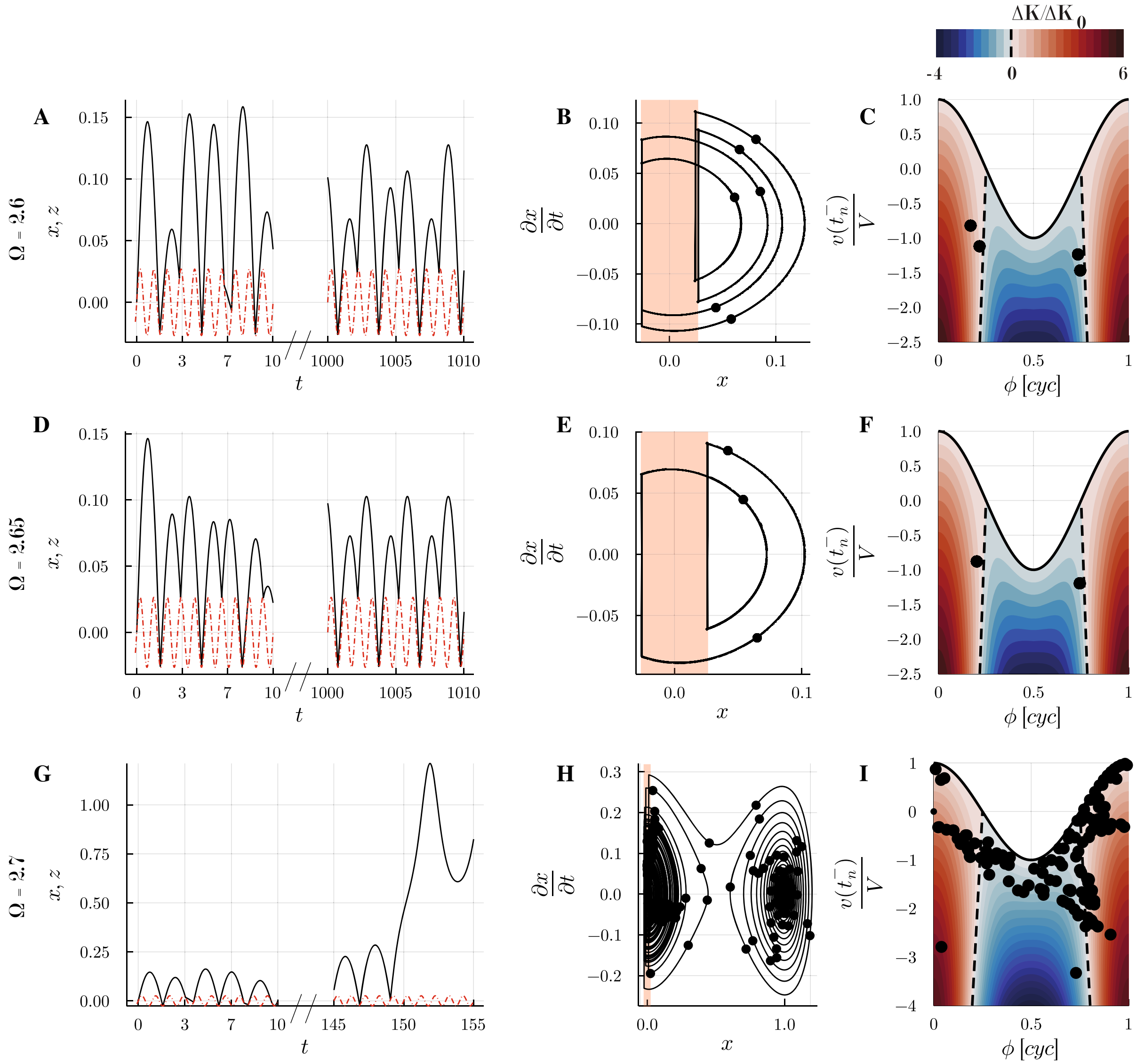

Fig. 5 Same as Fig. 4 but for higher excitation frequencies. Panels **h & i** include transient response. An intrawell to interwell bifurcation is observed with increasing frequency. As frequency increases, the response period decreases, and once sufficient energy is reached, the mass moves to the second equilibrium

of the monodromy matrix. The result of this analysis corresponds to the lines in Fig. 6c. The stable solutions are observed to overlap with the results from the direct simulations. The period-two and period-four bifurcations correspond to the loss of stability of the period-one and period-two solutions, respectively.

The chaotic response observed in Fig. 6a–b continues until a frequency near 2.55. Here, Fig. 6a indicates a period of six, while Fig. 6b indicates only four impacts. This means that there are some periods of excitation that do not have an impact in this period-six response. A similar pattern exists at the highest frequencies shown; the period-three response has only two impacts per period. At the highest frequencies shown, the mass moves to the second equilibrium, such that $x_{\max} = 1$.

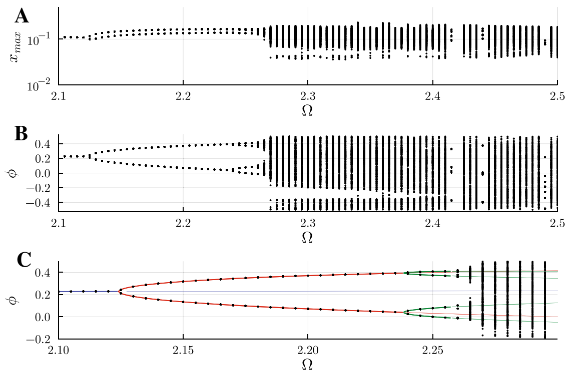

Fig. 6 Bifurcation diagram when Ω is used a control parameter while $V = 0.07$. **a** Maximum displacement of the mass within each cycle of the shaker displacement. **b** Phase of the impacts. Vertical red lines indicate values shown in Fig. 5c. Phase of impacts for Ω between 2.10 and 2.30. Continuous lines indicate predicted periodic responses described in Supplemental Information. Thick and thin lines correspond to stable and unstable solutions, respectively. Blue, red and green lines correspond to period-one, period-two and period-four solutions, respectively. As frequency increases, a series of period-doubling bifurcations occurs until a region of chaos is reached. At higher frequencies, stability is regained and the mass eventually exceeds the energy barrier and moves to the second equilibrium. (Color figure online)

3.3 Transition from intrawell response to interwell response as velocity amplitude varies

By modifying the other control parameter, the excitation velocity, V, another set of bifurcations occurs as the system shifts between interwell and intrawell responses. At $\Omega = 0.85$, these shifts are highlighted in Fig. 7. In Figs. 7a–c, at $V = 0.11$, a period-four intrawell response with five impacts per cycle is observed while the mass moves within the first energy well. As velocity increases to $V = 0.12$, the mass is able to escape the first energy well. Here, the escape occurs only during the transient response in Fig. 7d and quickly converges back to the period-eight intrawell response in Fig. 7e, forming a transient interwell response. This initial overshoot implies that this transition to interwell responses is dependent on initial conditions. Figure 7f shows the variety of impacts that the mass experiences as it converges to steady-state. As velocity continues to increase, the mass travels continuously between energy wells, which is shown in the continuous interwell responses of Figs. 7g–i with a period-one response and a single impact per cycle. Finally, at $V = 0.15$, the mass is able to escape the first equilibrium and remain in the second equilibrium after a single impact at $t = 0$, forming another type of transient interwell response.

These transitions are detailed in Fig. 8. At low velocity, a periodic response is observed. As excitation velocity increases, chaos is observed, then transient interwell responses before continuous interwell and finally back to transient interwell.

3.4 Classification of system dynamics

In addition to the targeted results described above, numerical simulations were run for a wide range of stimulus frequencies and amplitudes. The results of these simulations were used to classify the response according to the map in Fig. 9.

The three broad classes illustrated by the map include intrawell, transient interwell, and continuous interwell responses. The intrawell response, where the mass oscillates around its initial equilibrium configuration, tends to occur at low shaker velocity amplitudes. In these conditions, not enough energy is transferred to the mass in order to climb over the energy barrier. The mass then remains oscillating around the first equilibrium and never snaps through. At higher amplitude, the mass oscillates around both equilibria either continuously (continuous interwell response) or for finite duration before converging to the 2nd equilibrium (transient interwell). The shade of each cell corresponds to the response period. Since the energy added or removed from the mass during each collision is dependent on the relative phase of motion, the results shown here are only valid for this set of initial conditions.

Analytical equations were derived to approximate the boundary between the intrawell and transient interwell regions, which occurs between three analytical curves of interest: the single-impact threshold, the interwell threshold, and the quasi-static threshold. The single-impact threshold is an approximate upper limit for intrawell responses. Above this limit, the initial impact at $t = 0$ is sufficient to cause interwell motion because the kinetic energy given by Eq. (11) exceeds the energy barrier of the bistable spring, U_{cr} (see Fig. 1b). The single impact threshold in the shaker velocity amplitude is a constant value given by:

$$V_{\text{single impact}} = \frac{1}{4(1+e)} \tag{16}$$

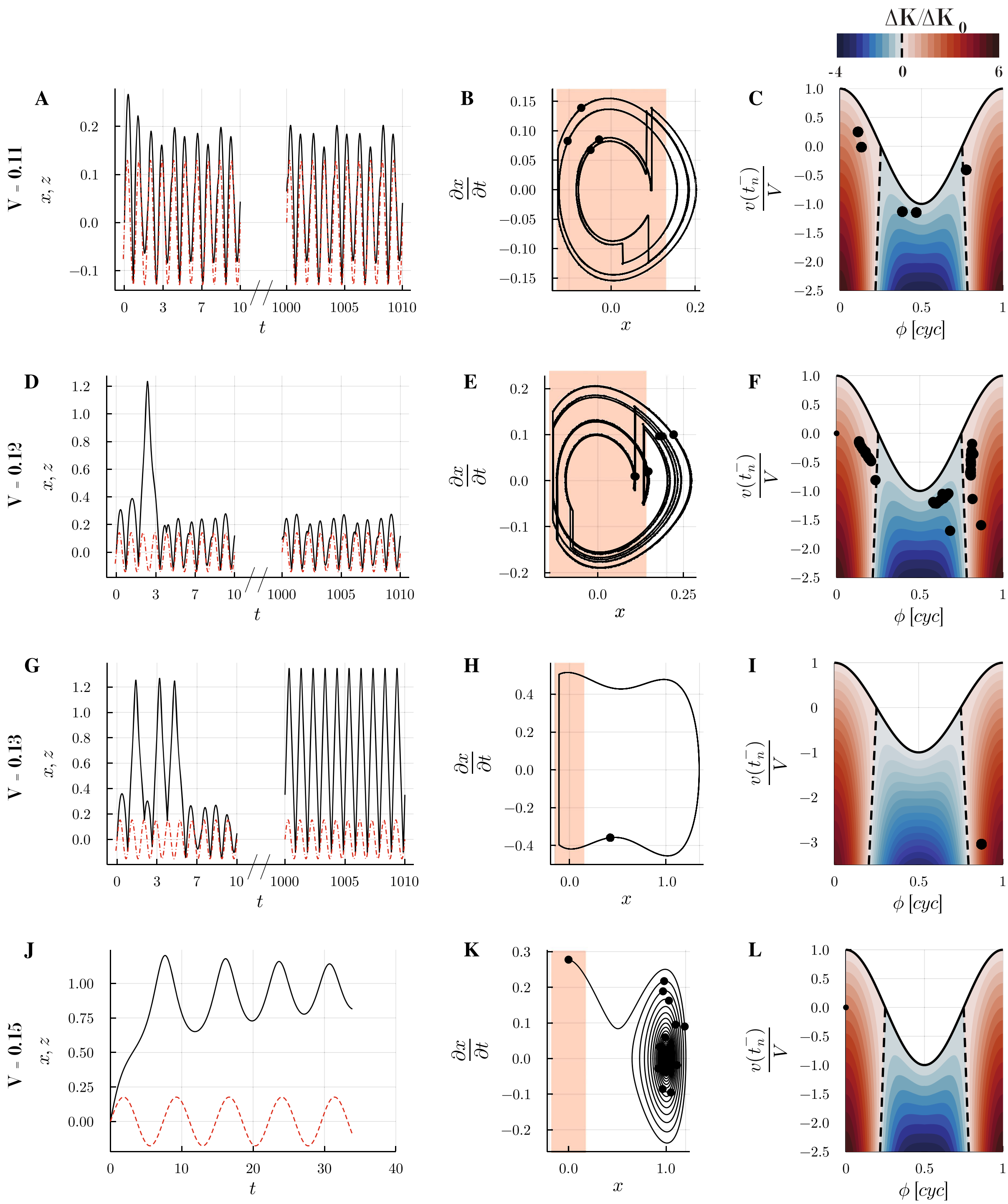

Fig. 7 Same as Fig. 5 for $\Omega = 0.85$ as velocity is increased. As velocity increases, a bifurcation from intrawell to interwell responses occurs

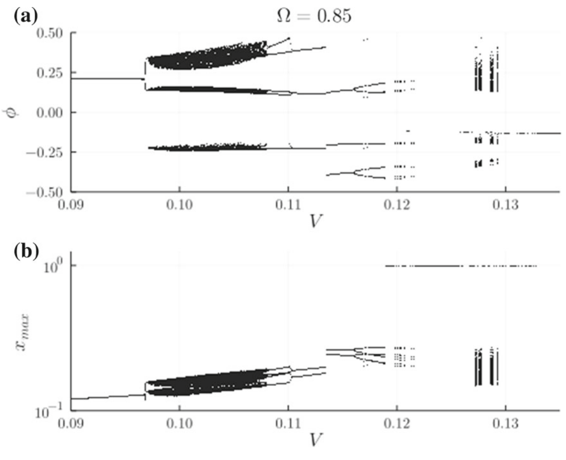

Fig. 8 Interwell bifurcation occurs with increasing velocity with $\Omega = 0.85$. Vertical lines indicate values shown in Fig. 7. At low velocities, the system is periodic. As velocity increases, the response period increases toward chaos. Finally, the mass travels to the second equilibrium in either transient or continuous interwell responses

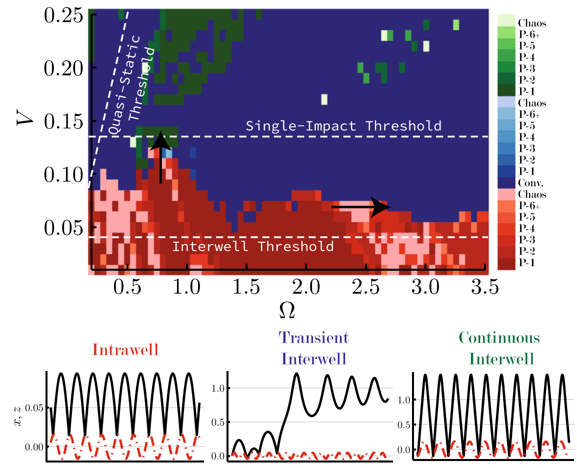

Fig. 9 By varying shaker amplitude and frequency, a wide range of responses are obtained. Red, blue, and green regions are stable periodic orbits that snap through zero, once, or multiple times, respectively. Lighter colors indicate a longer response period. The lightest regions of each color are chaotic responses. The darkest green and blue regions represent responses that converge to the second equilibrium. P-1, P-2,…, P-6+ correspond to periodic solutions of period 1, 2,…, 6+, respectively. The horizontal and vertical arrows correspond to the bifurcation diagrams shown in Figures 6 and 8, respectively. (Color figure online)

Examination of Fig. 9 confirms that all points above the line given by Eq. (16) are not interwell oscillations about Equilibrium 1 for the set of parameters. However, this equation neglects the effect of viscous damping, such that it is possible for intrawell responses to be observed slightly above this threshold as seen, for example, in Fig. 13 which is based on a lower coefficient of restitution ($e = 0.7$).

The interwell threshold is derived by considering a best-case scenario for maximum energy transfer to the mass and a series of approximations (see Supplemental Information). The following constant value for the interwell threshold is obtained:

$$V_{\text{inter}} = \frac{1}{2}\frac{1-e}{1+e} \tag{17}$$

As this conservative threshold describes an infinite set of collisions at ideal phase, all points below the line given by Eq. (17) are expected to be solely intrawell oscillations.

Finally, the quasi-static threshold curve is obtained by considering the response at the lowest frequencies. At the low frequency limit, the shaker must push the mass to the threshold quasi-statically, such that the amplitude of the shaker displacement must exceed the location of the energy barrier, $x_{cr} = 0.5$, to cause snapthrough. This analysis yields the following equation for the quasi-static velocity threshold:

$$V_{\text{quasi-static}} = 0.5 \times \omega, \tag{18}$$

which corresponds to the oblique dashed line shown in Fig. 9.

When no sticking occurs with low frequency excitation, many impacts occur per cycle of shaker movement. Since the higher number of impacts severely limits the phase shift possible before a grazing impact and thus source of chaos occurs, these responses may never converge to a periodic solution. One such example is shown in Fig. 10a, where the impact phase shifts slightly and aperiodically each cycle. At very low frequencies such as in Fig. 10b, the mass and shaker undergo a chattering sequence after which the two bodies remain in contact. As the shaker retracts, the mass separates and free vibration resumes. Since the conditions for separation are exactly the same for each cycle, once two sticking events occur, the response is guaranteed to be periodic with the same period as the excitation.

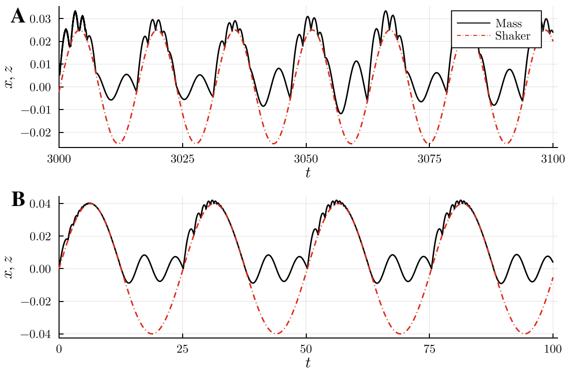

Fig. 10 Examples of waveforms observed at low frequencies. **a** A low frequency response without sticking, $V = 0.01$, $\Omega = 0.4$. **b** A low frequency response without sticking, $V = 0.01$, $\Omega = 0.25$

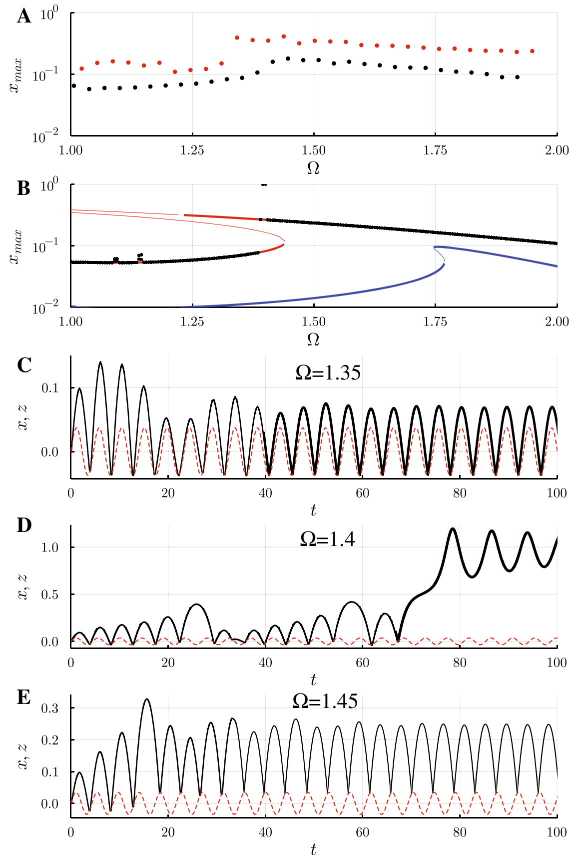

Fig. 11 **a** Maximum displacement of the mass within each cycle of the shaker displacement for calculated stable (thick lines) and unstable (thin lines) period-one solutions. Simulated results (dots) exactly match calculated values for $V = 0.005$ (black), $V = 0.03$ (red), and $V = 0.06$ (blue), except when the simulation results converge to a higher-period response or the second equilibrium in the $V = 0.06$ case. Nonlinear softening is clearly observed near $\Omega = 1.4$. **b–d** Examples of waveforms predicted around the peak of nonlinear resonance for $V = 0.05$. **c** A waveform that settles into a intrawell period-one response with excitation at $\Omega = 1.35$. **d** A response that converges to the second energy well after growing for several cycles with $\Omega = 1.4$. **e** Initial overshoot settling to a higher-energy period-one response with $\Omega = 1.45$. (Color figure online)

3.5 Analysis of the notch in the intrawell to interwell threshold

The theoretical results of Fig. 9 exhibit a notch that appears in the region of $\Omega \approx 1.2 - 1.6$, $V \approx 0.05 - 0.07$. While not as pronounced, the notch near $\Omega = 1.4$ is also visible in the theoretical results obtained with a lower e value shown in Fig. 13. This notch is caused by the combined effect of a nonlinear resonance of the steady-state response of the bistable system and of an overshoot in its transient response. At very low excitation amplitude, a maximum in the steady-state response is observed when $\Omega \approx 2$. In this condition, all impacts occur at a phase of 0, as discussed in Supplemental Information in the derivation of Eq. (17). As the shaker velocity amplitude is increased, the curve of the maximum displacement of the mass (Fig. 11a) veers toward the left due to the softening of the bistable spring [30], such that two stable branches and one stable branch are predicted for period-one solutions for $\Omega \approx 1.4$. The stable branch of low energy corresponds to impacts at a phase of approximately -0.25 cycles (i.e., minimum shaker displacement) while the branch of high energy corresponds to impacts at approximately 0.25 cycles (maximum shaker displacement). Figure 11b, d illustrates the convergence of responses to the low energy period-one orbit when $\Omega = 1.35$ and to the high energy period-one orbit when $\Omega = 1.45$, respectively. Both low-energy and high-energy stable period-one orbits exist when $\Omega = 1.4$ in Fig. 11d. However, the initial transient response tends to overshoot the steady-state solution in all cases for the initial conditions used in the simulations. In the case of $\Omega = 1.4$, this overshoot is sufficient to overcome the energy barrier of the bistable spring, such that a transient interwell response with convergence to the second equilibrium is observed.

4 Experimental observation of the nonlinear dynamics of the system

4.1 Experimental methods

We use the pendulum setup depicted in Fig. 12a–c to study the periodic and chaotic dynamics of a one-dimensional bistable system in experiment. The pendulum uses two ball bearings at its pivot point to ensure low friction and stable motion in the plane of oscillation, a lightweight wooden rod to act as the pendulum arm, and a 3D-printed housing that secures two vertically stacked neodymium (NdFe35) magnets at its end. Each of these magnets is 15.88 mm in diameter with a 0.79 mm thickness and 6.53 N pull force. Two additional neodymium magnets 15 mm under the pendulum bob determine the stable points in the potential energy. These magnets are spaced 28.19 mm apart with diameters of 25.4 mm, thicknesses of 1.59 mm, and pull forces of 30.19 N. The total length of the pendulum is 670 mm to reduce the pendulum's vertical displacement and maintain a small angle approximation.

A 3-dimensional finite element model that represents the experimental setup was analyzed in Ansys to validate its double-well potential energy. The natural frequency of the system around the equilibrium position can be determined by the effective moment of inertia around the pendulum pivot point and the equivalent torsional stiffness of the system (derivative of the torque due to both the gravitational and magnetic forces around the pivot point with respect to the angular displacement, θ). Specifically, Ansys Maxwell was used to analyze the magnetic interactions and obtain the torque induced on the pendulum due to the magnetic forces as a function of θ. With slightly modified coercivity value of 950 kA/m (6% increase from the default value for NdFe35 magnets), the natural frequency around the equilibrium position of the model was tuned to match the measured natural frequency in the experiments. The total potential energy of the system as the sum of the gravitational energy and elastic potential energy due to the magnetic interactions (integral of the torque due to magnetic forces) is plotted in Fig. 12d and is found to be nearly identical to the theoretical model of Eq. (1) near the two equilibria.

We use a portable shaker to impact the pendulum with varying displacement amplitudes and frequencies to observe the nonlinear vibroimpact dynamics of the bistable system in response to the shaker excitation.

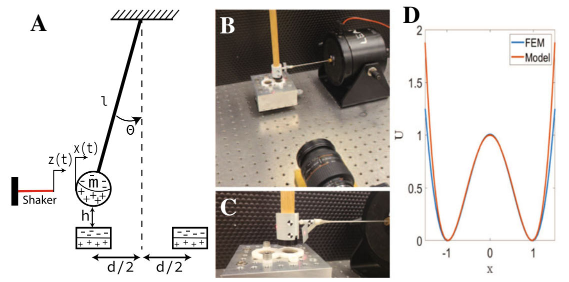

Fig. 12 **a** Experimental schematic. **b–c** Photograph of experimental apparatus. **d** Potential energy comparison between bistable model and theoretical pendulum

A high-speed camera with a tracking algorithm and two laser doppler vibrometers track the pendulum and shaker displacement and velocity, respectively.

4.2 Experimental results

For these series of tests, a series of measurements were obtained for a range of excitation velocities and frequencies. Due to shaker input limitations, this range appears as a wedge in Fig. 13. As in the theoretical results, both displacement amplitude and frequency are normalized by the separation distance of the equilibrium points (28.19 mm) and the natural frequency of the pendulum (3.08 Hz), respectively. Experimental results display a similar richness to the simulated results, with intrawell, transient interwell, and continuous interwell responses, as shown in Fig. 13. For direct comparison of theoretical results to experiments, the coefficient of restitution, e, was estimated to be 0.7 based on experimental observations of the velocity of the mass directly

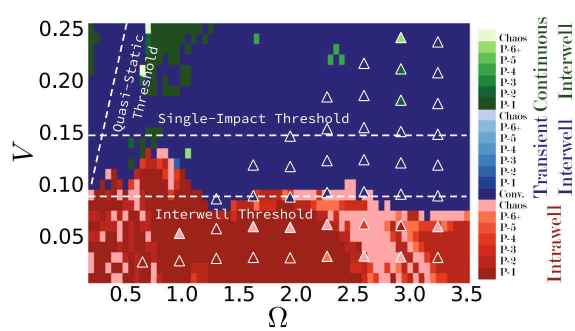

Fig. 13 Experimental (shaded triangles) and theoretical (colormap) results for the influence of shaker amplitude and frequency on the nonlinear dynamics of the system. $e = 0.7$ to match experimentally determined value. (Color figure online)

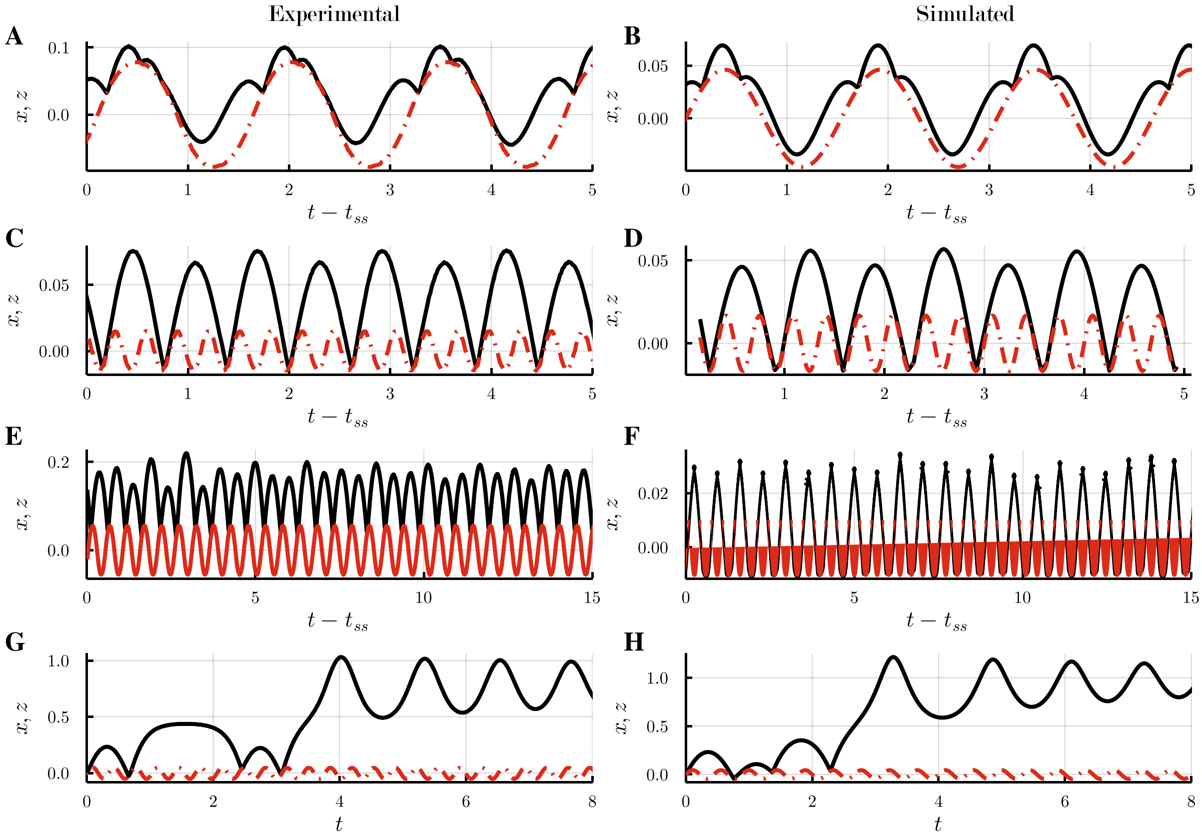

Fig. 14 Representative waveforms showing qualitative similarities between simulation and experiment. t_{ss} represents sufficient delay to reach a steady-state response. **a** Period- one intrawell, $\Omega = 0.649$, $V = 0.025$. **b** Period-one intrawell, $\Omega = 0.65$, $V = 0.03$. **c** Period-four intrawell, $\Omega = 3.247$, $V = 0.03$. **d** Period-four intrawell, $\Omega = 3$, $V = 0.05$. **e** Chaotic intrawell, $\Omega = 1.948$, $V = 0.059$. **f** Chaotic intrawell, $\Omega = 2.95$, $V = 0.03$. **g** Transient interwell, $\Omega = 2.922$, $V = 0.09$. **h** Transient interwell, $\Omega = 2.25$, $V = 0.1$

before and after collisions. Using this lower e value, the single-impact and interwell thresholds both increase. The interwell threshold increases faster than the single-impact threshold, so the transition region becomes narrower. Good qualitative agreement between model and experiments is observed in Fig. 13. A potential source of discrepancy between the model and experiments includes small unwanted motion outside the pendulum's plane of oscillation which originates from play present in the bearings and becomes more apparent for tests with high displacement amplitudes and high excitation frequencies. Nevertheless, by comparing numerical and experimental results in Fig. 14, we observe striking similarity in the waveforms observed in the period-one intrawell (Fig. 14a–b), period-four intrawell (Fig. 14c–d), chaotic (Fig. 14e–f), and transient interwell (Fig. 14g–h) responses. Recordings of these experiments can be found in Online Resources Movie_S1, Movie_S2, Movie_S3, and Movie_S4 in the Supplemental Information.

5 Conclusions

In this work, the fundamental problem of a bistable system excited by impacts with a sinusoidally vibrating shaker has been explored and found to have complex responses that are dependent on excitation parameters. Derivation of a dynamical model based on the coefficient of restitution allows for accurate simulation of these nonlinear dynamics. Using these computational models, we find that by varying excitation amplitude and frequency, several rich and distinct response regions can be obtained. These responses range from periodic to chaotic. Under low amplitude and low frequency excitation, the mass does not transition to interwell motion and remains around the first equilibrium. At higher frequency and/or amplitude, the mass may transition between energy wells once or repeatedly, depending on excitation parameters. The largest regions of stable periodic orbits are either high energy interwell responses or period-one intrawell responses.

Experimental results validate the presence of these rich dynamics and confirm the physical presence of intrawell periodic, intrawell chaotic, and transient interwell dynamics in a pendulum model.

Funding This study was supported by NSF Grant CMMI 2037565, the Georgia Institute of Technology Quantum Alliance, and the Woodruff Launch Seed Grant at Georgia Tech.

Data availability The data and source codes used in this work can be made available upon request to the corresponding author Julien Meaud (julien.meaud@me.gatech.edu).

Declarations

Conflict of interest The authors declare that they have no conflict of interest.

References

1. Shan, S., Kang, S.H., Raney, J.R., Wang, P., Fang, L., Candido, F., Lewis, J.A., Bertoldi, K.: Multistable architected materials for trapping elastic strain energy. Adv. Mater. **27**(29), 4296–4301 (2015)
2. Meaud, J.: Multistable two-dimensional spring-mass lattices with tunable band gaps and wave directionality. J. Sound Vib. **434**, 44–62 (2018)
3. Ramakrishnan, V., Frazier, M.: Multistable metamaterial on elastic foundation enables tunable morphology for elastic wave control. J. Appl. Phys. **127**(22), 225104 (2020)
4. Mann, B., Sims, N.: Energy harvesting from the nonlinear oscillations of magnetic levitation. J. Sound Vib. **319**(1), 515–530 (2009). https://doi.org/10.1016/j.jsv.2008.06.011
5. Harne, R.L., Wang, K.: A review of the recent research on vibration energy harvesting via bistable systems. Smart Mater. Struct. **22**(2), 023001 (2013)
6. Pellegrini, S.P., Tolou, N., Schenk, M., Herder, J.L.: Bistable vibration energy harvesters: a review. J. Intell. Mater. Syst. Struct. **24**(11), 1303–1312 (2013)
7. Yasuda, H., Buskohl, P.R., Gillman, A., Murphey, T.D., Stepney, S., Vaia, R.A., Raney, J.R.: Mechanical computing. Nature **598**(7879), 39–48 (2021)
8. Bilal, O.R., Foehr, A., Daraio, C.: Bistable metamaterial for switching and cascading elastic vibrations. Proc. Natl. Acad. Sci. **114**(18), 4603–4606 (2017)
9. Xia, Y., Ruzzene, M., Erturk, A.: Dramatic bandwidth enhancement in nonlinear metastructures via bistable attachments. Appl. Phys. Lett. **114**(9), 093501 (2019)
10. Raney, J.R., Nadkarni, N., Daraio, C., Kochmann, D.M., Lewis, J.A., Bertoldi, K.: Stable propagation of mechanical signals in soft media using stored elastic energy. Proc. Natl. Acad. Sci. **113**(35), 9722–9727 (2016)
11. Arrieta, A., Hagedorn, P., Erturk, A., Inman, D.: A piezoelectric bistable plate for nonlinear broadband energy harvesting. Appl. Phys. Lett. **97**(10), 104102 (2010)
12. Virgin, L.N.: Vibration of Axially-Loaded Structures. Cambridge University Press, Cambridge (2007)
13. Wang, K.-W., Harne, R.L.: Harnessing Bistable Structural Dynamics: For Vibration Control, Energy Harvesting and Sensing. John Wiley & Sons, London (2017)
14. Datseris, G., Parlitz, U.: Nonlinear Dynamics: A Concise Introduction Interlaced with Code. Springer Nature, Berlin (2022)
15. Luo, A.C., Han, R.P.: The dynamics of a bouncing ball with a sinusoidally vibrating table revisited. Nonlinear Dyn. **10**(1), 1–18 (1996)
16. Umeda, M., Nakamura, K., Ueha, S.: Analysis of the transformation of mechanical impact energy to electric energy using piezoelectric vibrator. Jpn. J. Appl. Phys. **35**(5S), 3267 (1996)
17. Babitsky, V.I.: Theory of Vibro-Impact Systems and Applications. Springer, Berlin (2013)
18. Luo, A.C., Guo, Y.: Vibro-Impact Dynamics. John Wiley & Sons, London (2012)
19. Ibrahim, R.A.: Vibro-Impact Dynamics: Modeling, Mapping and Applications, vol. 43. Springer, Berlin (2009)
20. Shaw, S., Holmes, P.: A periodically forced impact oscillator with large dissipation (1983)
21. Zhou, S., Cao, J., Inman, D.J., Liu, S., Wang, W., Lin, J.: Impact-induced high-energy orbits of nonlinear energy harvesters. Appl. Phys. Lett. **106**(9), 093901 (2015)
22. Gu, L., Livermore, C.: Impact-driven, frequency upconverting coupled vibration energy harvesting device for low frequency operation. Smart Mater. Struct. **20**(4), 045004 (2011)
23. Xie, Z., Kwuimy, C.K., Wang, T., Ding, X., Huang, W.: Theoretical analysis of an impact-bistable piezoelectric energy harvester. Eur. Phys. J. Plus **134**(5), 1–10 (2019)
24. Bezanson, J., Edelman, A., Karpinski, S., Shah, V.B.: Julia: a fresh approach to numerical computing. SIAM Rev. **59**(1), 65–98 (2017)
25. Rackauckas, C., Nie, Q.: Differentialequations.jl—a performant and feature-rich ecosystem for solving differential equations in Julia. J. Open Res. Softw. **5**(1) (2017)
26. Budd, C., Dux, F.: Chattering and related behaviour in impact oscillators. Philos. Trans. R. Soc. Lond. Ser. A. Phys. Eng. Sci. **347**(1683), 365–389 (1994)
27. Thompson, J., Ghaffari, R.: Chaos after period-doubling bifurcations in the resonance of an impact oscillator. Phys. Lett. A **91**(1), 5–8 (1982). https://doi.org/10.1016/0375-9601(82)90248-1
28. Peeters, M., Viguié, R., Sérandour, G., Kerschen, G., Golinval, J.-C.: Nonlinear normal modes, part ii: toward a practical computation using numerical continuation techniques. Mech. Syst. Signal Process. **23**(1), 195–216 (2009)

29. Sracic, M.W., Allen, M.S.: Numerical continuation of periodic orbits for harmonically forced nonlinear systems, In: Civil Engineering Topics, vol. 4, pp. 51–69. Springer, Berlin (2011)
30. Nayfeh, A.H., Balachandran, B.: Applied Nonlinear Dynamics: Analytical, Computational, and Experimental Methods. John Wiley & Sons, London (2008)